Superconductor Science and Technology

PAPER • OPEN ACCESS

Advances in Nb_3Sn superconducting radiofrequency cavities towards first practical accelerator applications

To cite this article: S Posen *et al* 2021 *Supercond. Sci. Technol.* **34** 025007

OPEN ACCESS
IOP Publishing
Superconductor Science and Technology
Supercond. Sci. Technol. **34** (2021) 025007 (10pp)
https://doi.org/10.1088/1361-6668/abc7f7

Advances in Nb_3Sn superconducting radiofrequency cavities towards first practical accelerator applications

S Posen[1], J Lee[1,2], D N Seidman[2,3], A Romanenko[1], B Tennis[1], O S Melnychuk[1] and D A Sergatskov[1]

[1] Fermi National Accelerator Laboratory, Batavia, IL 60510, United States of America
[2] Department of Materials Science and Engineering Northwestern University, Evanston, IL 60208, United States of America
[3] Northwestern University Center for Atom-Probe Tomography (NUCAPT), Evanston, IL 60208, United States of America

E-mail: sposen@fnal.gov

Received 4 August 2020, revised 27 October 2020
Accepted for publication 5 November 2020
Published 11 January 2021

Abstract

Nb_3Sn is a promising next-generation material for superconducting radiofrequency cavities, with significant potential for both large scale and compact accelerator applications. However, so far, Nb_3Sn cavities have been limited to continuous wave accelerating fields <18 MV m^{-1}. In this paper, new results are presented with significantly higher fields, as high as 24 MV m^{-1} in single cell cavities. Results are also presented from the first ever Nb_3Sn-coated 1.3 GHz 9-cell cavity, a full-scale demonstration on the cavity type used in production for the European XFEL and LCLS-II. Results are presented together with heat dissipation curves to emphasize the potential for industrial accelerator applications using cryocooler-based cooling systems. The cavities studied have an atypical shiny visual appearance, and microscopy studies of witness samples reveal significantly reduced surface roughness and smaller film thickness compared to typical Nb_3Sn films for superconducting cavities. Possible mechanisms for increased maximum field are discussed as well as implications for physics of RF superconductivity in the low coherence length regime. Outlook for continued development is presented.

Supplementary material for this article is available online

Keywords: superconducting radiofrequency, particle accelerators, Nb_3Sn

(Some figures may appear in colour only in the online journal)

1. Introduction

Superconducting radiofrequency (SRF) cavities are widely used for particle beam acceleration because of their ability to generate large amplitude accelerating electric fields (E_{acc}) with small heat dissipation (P_d). Niobium has been the material of choice for SRF cavities for decades, having the highest critical temperature (T_c) of the elements, ~9.2 K, allowing it to have a high quality factor Q_0 (small P_d) at temperatures accessible with liquid helium, with typical> operation ~2 K. Nb_3Sn is a new SRF material that is being explored, with significantly higher T_c (~18 K) than Nb (~9 K), which has allowed it to achieve higher Q_0 than Nb in a wide temperature range [1]. However, Nb_3Sn cavities have been limited to continuous wave (cw, i.e. not pulsed) accelerating gradients

significantly smaller than Nb, with the best cavities being limited by quench (loss of superconductivity) at 18 MV m^{-1}, compared to the best Nb cavities reaching up to ∼50 MV m^{-1} [2]. Furthermore, larger Nb_3Sn cavities—cavities with more than two cells or with frequency below ∼1 GHz—have in past research programs had limited development and relatively poor performance in the small number of tests performed on them, generally limited to ∼5 MV m^{-1} [3, 4].

Development of Nb_3Sn to overcome these limitations is motivated [5, 6] partially by theoretical predictions of higher maximum fields if the films are sufficiently optimized [7] and partially by the ability to operate at higher temperatures where cryogenic efficiency is far higher[4] [8]. In addition to the potential for large scale applications, researchers are developing cryocooler-based cooling schemes [9–11] to enable compact accelerator applications based on Nb_3Sn cavities operating at ∼4 K for small- and medium-scale applications such as wastewater treatment and medical isotope production.

Achieving a uniform stoichiometry over the RF surface of an SRF cavity is significantly more complex with Nb_3Sn than with Nb. The superconducting properties of Nb-Sn compounds vary with composition, and there is a narrow composition range around 25% Sn with the highest T_c [12]. There are a number of methods to create Nb_3Sn, but so far, the method that has been most successful in terms of cavity performance is vapor diffusion [4, 13, 14]. Vapor diffusion takes advantage of the phase diagram at high temperatures to 'phase-lock' to the desired composition (as described in [15]). This technique is now used by several labs around the world for coating cavities with Nb_3Sn [1, 16, 17]. Researchers continue to optimize the process through a combination of coating parameter space exploration, cryogenic RF measurement, microstructural analysis, and materials science. There has been significant recent progress in understanding detrimental microstructural imperfections that can occur in vapor diffusion Nb_3Sn coatings, including abnormally large thin grains (so-called 'patchy' regions) [18–20] and grain boundaries (GBs) with segregated tin [21]. It has been demonstrated that these imperfections in Nb_3Sn can be minimized by carefully selecting growth parameters.

In this paper, we report on experiments exploring modifications to typical coating procedures to make films that have relatively low surface roughness and relatively small film thickness. Reducing surface roughness may augment the energy barrier to flux penetration and therefore increase the quench field [22]. Thinner films may have higher quench field due to the poor thermal conductivity of Nb_3Sn, $\sim 10^3$ lower than that of Nb [23], for example by improving stability in the case of localized defects. We show measurements of several types of SRF cavities with smooth, thin films, showing significantly improved performance compared to the previous state-of-the-art.

[4] E.g. a large cryogenic plant has a coefficient of performance approximately 3–4 times better at 4.4 K vs 2 K.

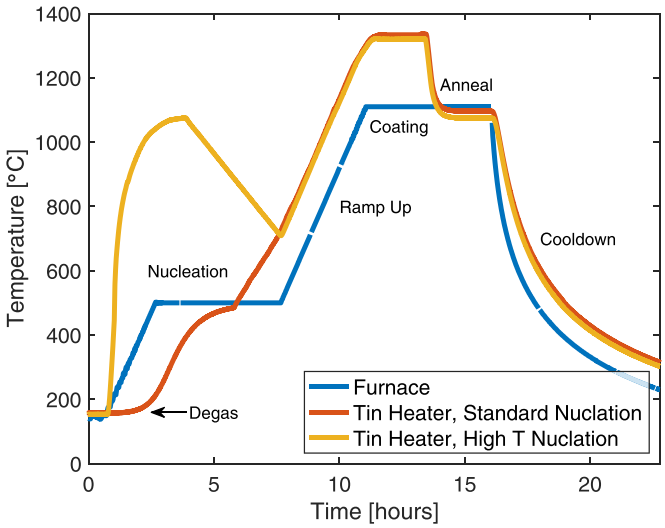

Figure 1. Vapor diffusion coating process at Fermilab with standard nucleation step at ∼500 °C and with modified high-temperature nucleation step. The blue curve for the furnace temperature applies for both nucleation types.

2. Nb_3Sn coating process development

A typical vapor diffusion Nb_3Sn coating procedure is shown in the top of figure 1. The process involves six stages (described in more detail in [1]):

(a) Degas at ∼140 °C—allows ramp up to proceed without large pressure spikes. Typical duration ∼24 h (not shown in figure 1).
(b) Nucleation at ∼500 °C—$SnCl_2$ has a high vapor pressure in this temperature range and creates Sn sites on the surface
(c) Ramp up—furnace is ramped up to coating temperature ∼1100 °C. Sn heater is used to maintain the Sn source ∼100 °C–200 °C hotter than the furnace to maintain high vapor pressure.
(d) Coating at ∼1100 °C—Sn evaporates and reacts with the Nb of the substrate to form Nb_3Sn
(e) Anneal at ∼1100 °C—the Sn heater is turned off but the furnace is maintained at temperature to give a chance for excess Sn on the surface to evaporate or diffuse
(f) Cooldown

Steps 2 and 3 to maintain high vapor pressure were recommended by Hillenbrand *et al* [5] and a proposed explanation for the benefit provided by the high vapor pressure is reducing the formation of anomalously large thin grains [20].

Procedures for producing low surface roughness, thin Nb_3Sn coatings are not yet well established and repeatable. Smooth, thin films have been produced several times at Fermilab, and in this paper, we will present results from them, but additional studies are needed to fully understand which coating parameters are key determinants for these properties. However, we can identify several common features among coating procedures that have produced smooth, thin films:

- The niobium cavity substrates were given electropolish treatment (as opposed to buffered chemical polish) to achieve a smooth surface prior to coating
- The niobium substrates were anodized to 30 V in ammonia prior to coating (recommended previously, e.g. [5] and [24])
- To encourage high vapor pressure, the Sn heater was driven with maximum power available (measured ∼1300 °C in thermocouples in heater coil, expect somewhere between 1200 °C and 1250 °C in Sn crucible based on previous calibration)
- To encourage high vapor pressure, a relatively large crucible diameter was used (∼15 mm or larger)
- To prevent condensation of Sn droplets on the surface due to a high vapor pressure in a closed volume, one or more ports of the cavity were kept open to the chamber (similar to the Cornell setup [1])
- The nucleation step was substantially modified, to have a rapid ramp to high temperatures ∼1000 °C—this will be discussed in detail below
- A nitrogen infusion step was added at the end of the coating process—this is also discussed in detail below

The high temperature nucleation step is illustrated in the yellow curve of figure 1. Immediately following the degas, while the furnace temperature begins a slow ramp to 500 °C, the Sn source heater is driven with high power to raise its temperature very quickly, achieving eventually a maximum temperature of ∼1000 °C. The heater raises the temperature of two crucibles, one that contains Sn and one that contains $SnCl_2$. The vapor pressure of the Sn is still expected to be relatively low at these temperatures, but the $SnCl_2$ is expected to have a very high vapor pressure [25]. It is expected that the full quantity of $SnCl_2$ will evaporate very quickly, much faster than it would during the other process shown in the red curve of figure 1, especially considering the observed thermal lag of the unpowered Sn heater relative to the furnace. The goal of the high temperature nucleation step is to create a very high vapor pressure to (a) reduce the mean free path of the vapor and thereby improve homogeneity over the surface, and (b) rapidly transport Sn to the surface early in the process (see [20, 26]).

The nitrogen infusion step was added in an attempt to raise maximum gradients as has been demonstrated in niobium cavities [27]. Once the furnace temperature has dropped to 120 °C, that temperature is maintained for 48 h, and nitrogen gas is bled into the furnace, maintaining ∼25 mtorr of pressure (see figure 2). In niobium cavities, this process creates nitrogen interstitials in the near surface, and it is hypothesized that the resulting 'dirty' layer in the superconductor enhances the energy barrier preventing flux entry into the superconductor. Nb_3Sn has intrinsically a much shorter coherence length than Nb, but depending on the mean free path, it can be clean (as was previously observed for vapor diffusion films [28]) or dirty [29], and calculations suggest that a dirty layer is will create a significant enhancement of the maximum field compared to a clean layer [30]. While it was not expected that nitrogen would diffuse in the same way in Nb_3Sn that it does in Nb, it

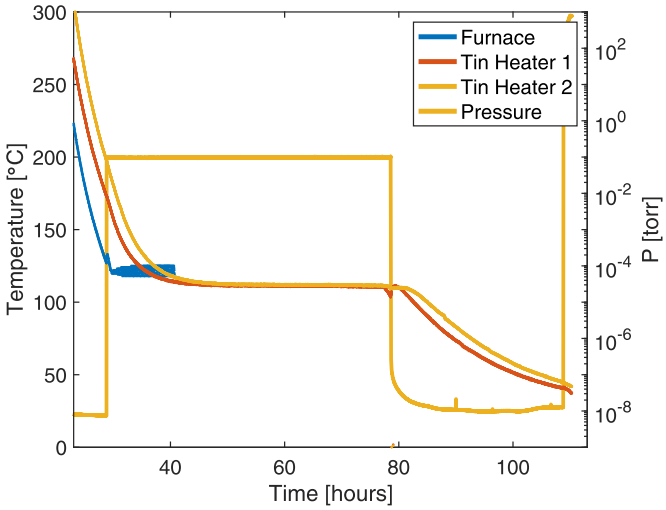

Figure 2. Example of a N-infusion step after Nb_3Sn coating.

was decided attempt to use the same procedure as used on Nb as a first evaluation.

A number of coatings were performed, varying parameters described above as well as others such as tin quantities. In all cases, cavities were evaluated at least visually, and sometimes also with cryogenic testing. Visual evaluation would often give useful indications of coating quality. Examples include patterns of dark spots (interpreted as tin condensation) [20], local shiny spots (interpreted as anomalously large thin grains), and a shiny, almost glossy appearance over the whole surface (interpreted as a low surface roughness coating).

Recently, some repeatability has been established in generating shiny, glossy films by reducing the quantity of tin in the coatings substantially (by ∼50%). Providing less tin from the source would be consistent with the films being thinner. However, this reduction of tin quantity was not implemented for the first shiny coatings produced at Fermilab, so it is not clear if it is a requirement. The recent repeatable shiny films have not been evaluated with cryogenic testing due to limitations caused by the COVID-19 pandemic. This will be a focus of future paper; in this work we will focus on the results already obtained.

3. Microscopy of Nb_3Sn coatings

Nb_3Sn samples were analyzed using optical, laser confocal microscope, scanning electron microscope (SEM), and high-angle annular dark-field (HAADF) scanning transmission electron microscopy (STEM). Surface roughness was characterized using Bruker ContourGT Optical profiler. SEM imaging of Nb_3Sn samples was performed using FEI Quanta SEM with 30 kV electron beam and TEM analyses was performed using Hitachi HD 2300 electron microscopes with 200 kV electron beam. Cross-sectional TEM samples of Nb_3Sn coatings on Nb were prepared by FEI Helios Nanolab 650 focused ion beam.

Typically, Nb_3Sn vapor diffusion coatings have a matte, nonreflective gray visual appearance. However, the cavities

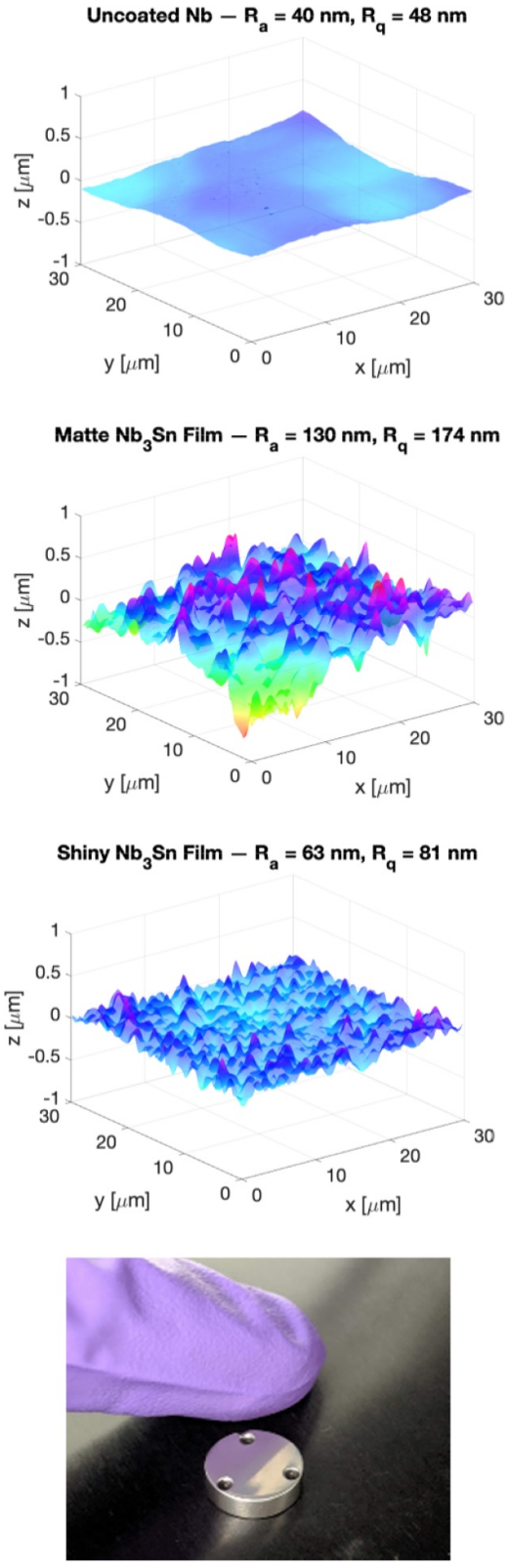

Figure 3. Comparison of surface roughness (represented by arithmetic mean and root mean squared deviation R_a and R_q) of three samples: electropolished niobium sample before coating (top), a coating typical of previous matte Nb_3Sn (second from top), and a new shiny Fermilab Nb_3Sn-coated sample (second from bottom). A photo shows the shiny Nb_3Sn sample surface reflecting a gloved finger (bottom).

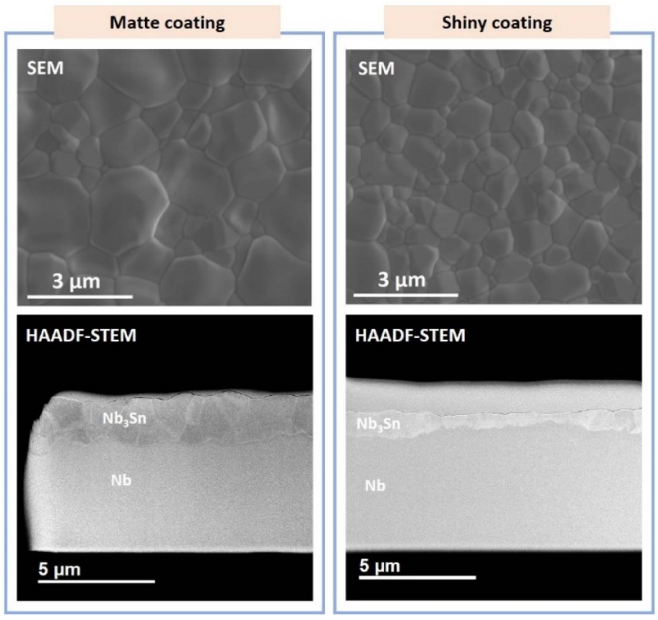

Figure 4. Plane-view SEM and cross-sectional HAADF-STEM image of Nb_3Sn coatings on Nb. The shiny Nb_3Sn coating is thinner ($\sim$1 μm) and has smaller grain diameter ($< \sim$1 μm) than the matte Nb_3Sn coating. Platinum layers are visible on the top of Nb_3Sn coating in the HAADF-STEM images. The Pt was deposited during the TEM sample preparation to protect the surface of the Nb_3Sn coatings.

studied in this paper had a shiny, reflective appearance immediately noticeable upon removal from the furnace. Witness samples coated with the cavities also show a shiny appearance, and surface roughness measurements via laser confocal microscope show a significantly smoother surface than typical coatings, consistent with the shiny appearance. This is illustrated in figure 3.

Figure 4 compares the microstructure of a matte Nb_3Sn coating and that of a shiny Nb_3Sn coating, both plane-view and in cross-section. It shows that the shiny Nb_3Sn coating is thinner ($\sim$1 μm) than the matte Nb_3Sn coating ($\sim$2 μm). Also, its grain diameter is smaller (0.93 ± 0.30 μm) than the matte Nb_3Sn coating (1.37 ± 0.57 μm).

Surface roughness values of various Nb_3Sn coatings prepared by standard and new coating procedures are measured by optical microscopy and summarized in figure 5. It demonstrates that the surface roughness of the Nb_3Sn coatings is strongly correlated to the film thickness and average diameter of Nb_3Sn grains: thinner coatings have smaller grain size and smaller surface roughness. The correlation among film thickness, grain size and surface roughness is generally observed and reported in other thin film coatings [31, 32]. Smaller grains typically have less height variation within each grain (consistent with their smaller size), leading to lower surface roughness.

Typical matte Nb_3Sn coatingsS are $\sim$2 μm thick with $\sim$1.5 μm grain diameter, and more than $\sim$150 nm of surface roughness (R_a) values, measured in a 47 μm by 62 μm area. The shiny Nb_3Sn coatings are thinner, $\sim$1 μm, have smaller

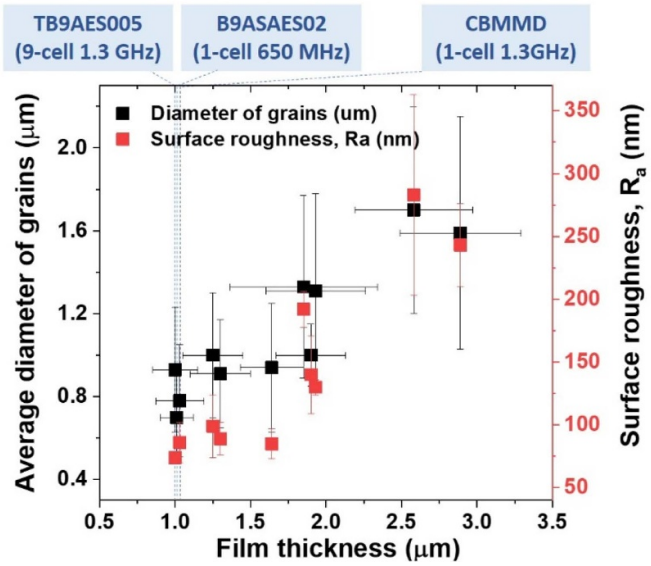

Figure 5. Correlation among film thickness, average diameter of Nb_3Sn grains, and surface roughness of Nb_3Sn coatings on Nb: it clearly shows that surface roughness is roughly proportional to the film thickness and average grain diameter of Nb_3Sn coatings.

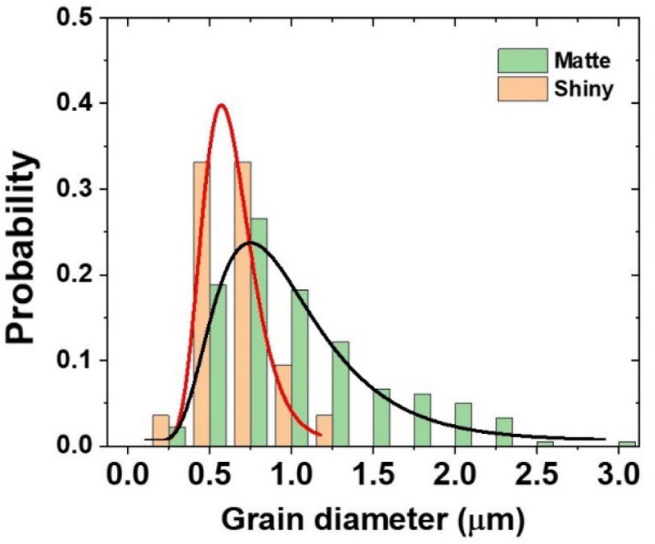

Figure 7. Histogram of grain size distribution in matte and shiny Nb_3Sn coatings: it reveals wider distribution of Nb_3Sn grains in the matte ($\sigma = 0.25$) compared to the shiny coating ($\sigma = 0.45$), where σ is standard deviation assuming they follow log-normal distribution.

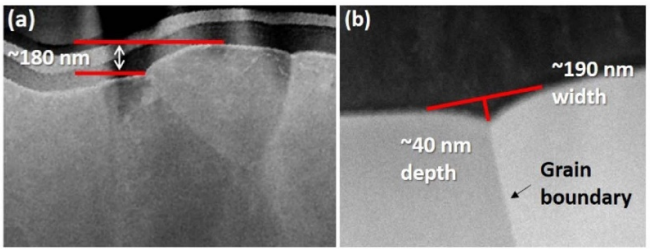

Figure 6. HAADF-STEM images illustrate the causes of surface roughness in a matte Nb_3Sn coating: (a) height differences across grains, ∼180 nm, and; (b) groves at grain boundaries (GBs) with ∼190 nm width and ∼40 nm depth.

grain diameter, less than ∼1 μm, and have surface roughness as low as $R_a \sim 80$ nm. A previous study performed by adjusting coating temperature and duration showed a similar general relationship between film thickness, grain size, and surface roughness [33]. The effect of these factors on Nb_3Sn cavity performance is presented and discussed in sections IV and V.

HAADF-STEM images in figure 6 display the height differences among grains as well as grooves at GBs in a sample of matte Nb_3Sn. Height differences ∼180 nm between Nb_3Sn grains are observed as well as grooves at GBs ∼ 40 nm deep with ∼190 nm width. As expected, comparative analyses between the surface profiles measured by optical microscope and HAADF-STEM images of the surface morphology of Nb_3Sn coatings indicate that the height differences among Nb_3Sn grains (∼200 nm) and grooves (∼40 nm) are the primary cause of surface roughness of Nb_3Sn coatings. This is consistent with smaller grain size leading to improved surface roughness.

We also note that the shiny coating has a narrower grain size distribution. Figure 7 displays histograms of grain diameters in two Nb_3Sn coatings: (a) matte and; (b) shiny. The matte Nb_3Sn coating shows a wide distribution of grain diameter from 300 nm to 3 μm. In contrast, the shiny Nb_3Sn coatings show a narrow distribution of grain diameter around ∼700 nm. The size distributions of Nb_3Sn grains are normalized and fit with log-normal distributions. The shiny Nb_3Sn coating displays significantly smaller standard deviation ($\sigma = 0.25$) compared to the matte coating ($\sigma = 0.45$).

Compositional analysis was performed on a witness sample coated with single cell 1.3 GHz cavity CBMM-D using secondary ion mass spectrometry (SIMS). The nitrogen-treated sample did *not* show a significant excess of nitrogen in the near surface compared to witness samples that did not receive a nitrogen infusion step. Figure 8 contrasts this with a N-infused Nb sample, that shows an excess of N relative to an EP'd sample, several nm into the near surface, below the oxide. It is therefore unclear if the nitrogen infusion step had any effect, but after observing strong RF performance in CBMM-D, it has typically been included in an effort to maintain consistency while trying to reproduce its coating procedure. Additionally, several coatings were attempted with the N-infusion step that resulted in Nb_3Sn layers that were not smooth, shiny, or thinner than ∼2 μm, suggesting that this step was not the key factor for resulting in these qualities.

A study of the effect of the high-temperature nucleation step on the microstructure of Nb_3Sn coatings is presented in supplemental material A (available online at stacks.iop.org/SUST/34/025007/mmedia). The study finds that the coverage of Sn nucleation islands is denser and somewhat more uniform after high temperature nucleation, and with larger islands than in the standard nucleation. This is expected to reduce the formation of 'patchy' regions on the surface [20]. The high density of nucleation sites may also contribute to the smaller grain size in the final film.

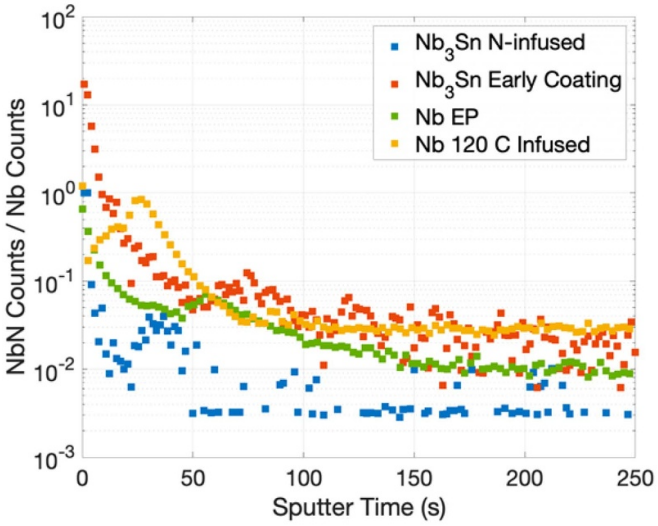

Figure 8. Depth profile of nitrogen in various samples, measured by SIMS. Signals are normalized to Nb counts. Sputtering rate is approximately 0.1 nm s^{-1}.

4. Performance of Nb_3Sn SRF cavities

The performance of the cavities is evaluated in a vertical test cryostat using typical cavity RF measurement procedures (e.g. see [34]). Cavities are cooled slowly and uniformly through the critical temperature ∼18 K to prevent degradation due to trapped thermocurrents [4]. Cancellation coils are used to minimize the ambient field around the cavities to ∼1 mG or smaller. Tests are usually performed with slightly pressurized liquid helium at 4.4 K and with subatmospheric superfluid ∼2 K. Measurements are also sometimes performed in cold helium gas to evaluate performance at higher temperatures for cryocooler-based applications.

Several cavities with the shiny film appearance were tested in liquid helium in Fermilab's vertical test stand (VTS): a single cell 1.3 GHz cavity CBMM-D, a single cell 650 MHz cavity B9AS-AES-002, and two 9-cell 1.3 GHz cavities, TB9ACC014 and TB9AES005. The performance of CBMM-D is shown in the top of figure 9. It reached 22.5 MV m^{-1} in the first VTS test, a new cw accelerating gradient record for Nb_3Sn cavities, which previously have been limited to ∼18 MV m^{-1}.

The gradient limit was quench, and there were indications that the quenching might be caused by multipacting. The quench field varied somewhat from cooldown to cooldown but consistently occurred in the multipacting band for a cavity of this type [36]. Temperature mapping and second sound measurements indicated that the quench was highly localized at the equator by polar angle, but widely spread around the cavity azimuthally (see supplemental material for details). To evaluate if it would be possible to process through the possible multipacting, the cavity was reassembled with an antenna with stronger coupling (to better match the cavity after unusually strong Q_0 degradation after quench) and retested at VTS. The cavity was quenched repeatedly by applying ∼100 W of forward power. This resulted in an increase in the maximum field

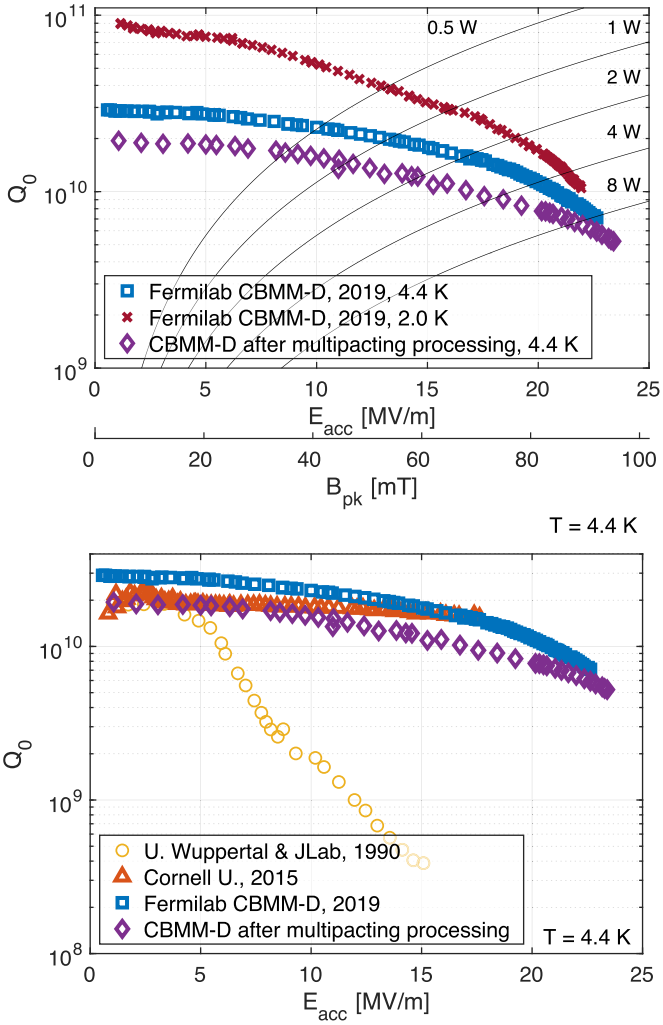

Figure 9. Performance of 1.3 GHz single cell cavity CBMM-D before and after processing (top) and comparison to a selection of previous 1.3–1.5 GHz single cell cavities (data from [24, 35]) at 4.4 K (bottom).

of the cavity. The cavity was thermal cycled after processing, reaching a maximum gradient of 24 MV m^{-1}. The 4.4 K curve is also plotted in the bottom of figure 1 and compared to some previous record Nb_3Sn cavity performances (all single cell cavities with frequency close to 1.3 GHz).

The 650 MHz cavity B9AS-AES-002 performed similarly, as shown in figure 10. It also showed multipacting-like behavior at ∼9 MV m^{-1}, but without quench. After processing through the multipacting, the cavity achieved a maximum accelerating gradient of 20 MV m^{-1}, limited by quench. At the maximum field, the cavity showed a Q_0 above 10^{10} at 4.4 K. The dissipated power at 10 MV m^{-1} is just 1.1 watts at 4.4 K, well within the range of large capacity cryocoolers, demonstrating the potential of coatings with this quality for compact accelerator applications. The performance is substantially improved compared to the limited experience reported in the literature of Nb_3Sn cavities with frequency <1 GHz [3].

Following the strong performance of these two cavities, a 9-cell 1.3 GHz cavity, TB9ACC014 was coated. This is the

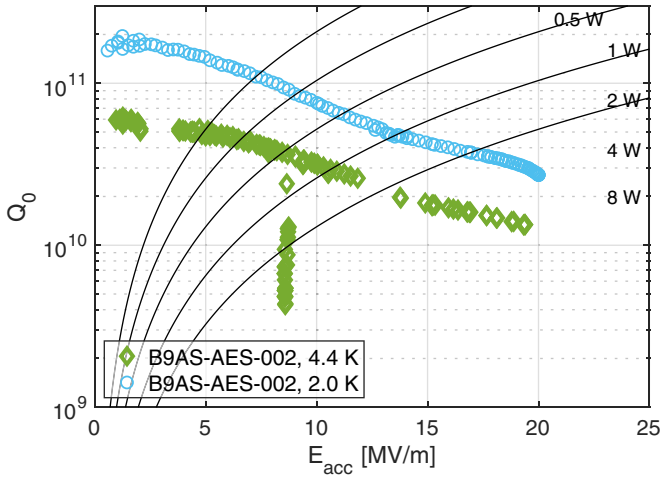

Figure 10. Performance of 650 MHz single cell cavity B9AS-AES-002. The multipacting at 9 MV m^{-1} was processed during the test.

first time a cavity of this type has been coated with Nb_3Sn. 9-cell 1.3 GHz cavities are practical accelerator structures ∼1 m in length used in state-of-the-art facilities such as the European XFEL and LCLS-II [37, 38]. They are much larger than the single cell cavities typically used in R&D. There is only a small number of past reports of Nb_3Sn multi-cell cavities produced via the vapor diffusion coating process, and with limited success in achieving uniform coatings over the length of the structure [4]. For TB9ACC014, it appears that the coating was sufficiently uniform for good performance, as shown in the performance curves at 1.5 K and 4.4 K in figure 11 (note that the plot includes a 0.8 nΩ correction for losses from each of the stainless steel flanges). While not as strongly performing as the single cell cavities, it shows significant progress towards making Nb_3Sn coatings practical for applications. This result is comparable to concurrent efforts by Eremeev *et al* on a pair of 5-cell 1.5 GHz cavities, which are smaller in size, but have obtained higher maximum gradients in vertical test [39].

Performance curves were also measured at higher temperatures with cooling from cold helium gas. The temperature stability was much less precise than with liquid cooling—figure 11 shows several curves and the corresponding temperature range measured by sensors attached to the outside surface of the cavity. Measuring Nb_3Sn cavities at higher temperatures is useful for developing an optimum operating temperature, which may be significantly higher than for niobium. If cryocoolers are used for cooling, for some types of cavities (e.g. at low frequencies), the optimal temperature may be above 4 K.

TB9ACC014 was electropolished and coated a second time. Its performance after the second coating was very similar to that in the first coating, as shown in figure 12. This may suggest a defect in the substrate being the performance limit. Considering this possibility, a second 9-cell cavity was coated, TB9AES005. This cavity had even higher maximum field than TB9ACC014, reaching above 15 MV m^{-1} before quench, with a Q_0 of 9×10^9 at 4.4 K. Its performance is also plotted in

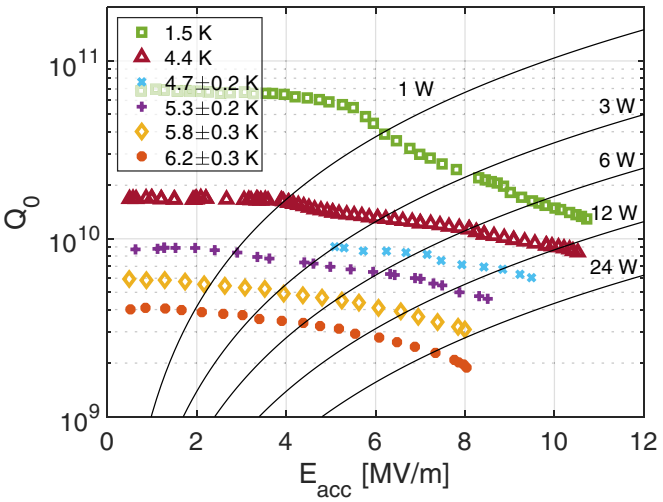

Figure 11. Top: inner surface of the 9-cell 1.3 GHz cavity TB9ACC014. Bottom: performance measured at 1.5 K and 4.4 K in liquid helium and at higher temperatures in cold helium gas (bottom).

figure 12 (includes stainless steel flange correction). The bottom of the figure plots the data at 1.5 K (TB9ACC014 test 1) or 2.0 K (TB9ACC014 test 2 and TB9AES005). They are plotted together because typically for our 1.3 GHz Nb_3Sn cavities, BCS resistance (i.e. temperature dependent component of the surface resistance [34]) at 2.0 K is small compared to residual resistance, so the Q vs E curves at these two temperatures are very similar. On the other hand, note that the residual resistance does not dominate at 4.4 K, as evidenced by the improvement in Q_0 at 2.0 K. In previous studies of Nb_3Sn cavities with frequency ∼1 GHz, residual has dominated at 4.4 K in some cases [28], but not others [35, 40].

5. Discussion

The cavity performance presented in the results section is unprecedented for cavities made with SRF materials beyond

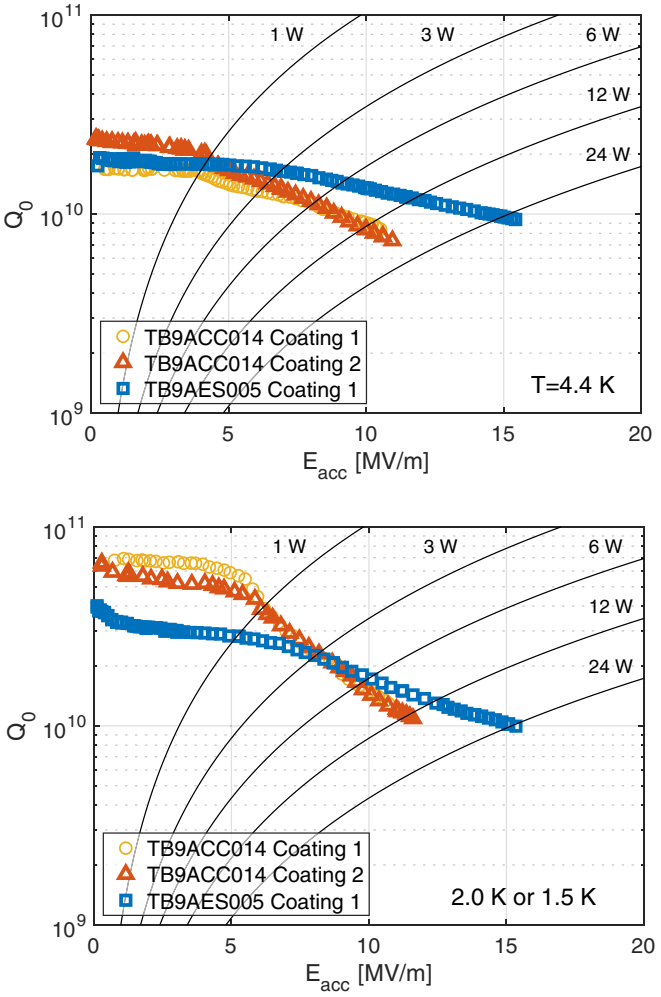

Figure 12. Vertical test performance of Nb_3Sn coated 9-cell cavities TB9ACC014 and TB9AES005. Curves were measured at 4.4 K (top) and 2.0 K or 1.5 K (bottom). Though all three coatings had very similar parameters, TB9AES005 has superior performance, suggesting a possible substrate dependence.

Nb. This includes two single cell Nb_3Sn cavities with cw accelerating gradients of 20 and 24 MV m^{-1}, significantly exceeding the previous highest value of 18 MV m^{-1} [1]. It also includes two 9-cell 1.3 GHz Nb_3Sn cavities, which reached 11 and 15 MV m^{-1}, an important demonstration on cavities typical of those used in applications. Even close to the maximum gradient, each of these cavities maintained a Q_0 on the order of 10^{10} at 4.4 K.

Each of these cavities had a shiny surface, not typically seen in Nb_3Sn SRF coatings. It seems likely that this is linked to the strong performance, and additional measurements will be performed in the future to evaluate this possibility. There are reasons to expect that the shiny coatings would improve performance. Microstructural analysis shown in figures 3 and 5 reveal that the shiny coatings are correlated with lower surface roughness. Surface roughness is caused by grooves and height differences between grains, figure 6, and it is suppressed with the smaller grain sizes observed in shiny films. Surface roughness can cause field enhancement and lowering of the energy barrier, causing penetration of magnetic flux at fields lower than the superheating field [22], meaning that a smoother layer may reach higher fields, depending on the type of geometric defects present. This is supported by calculations, simulations, and experiment, e.g. [41–45]. Analyses shown in figures 4 and 5 reveal that the shiny coatings are also correlated with a thinner layer. Nb_3Sn has significantly lower thermal conductivity than Nb [23, 46], so a thinner layer may be helpful for preventing thermal runaway, helping to stabilize the temperature on the inner surface, especially at local defects.

Nb_3Sn cavities can be thermally stable even with large amounts of dissipation over the surface, e.g. ∼30 W over a single cell cavity [47]. Consider for example, the case of CBMM-D described in the supplemental material, for which local thermometry measured a temperature increase as high as ∼0.5 K after quench (temperature increase is expected to be caused by flux trapped during the quench). However, before quench, the maximum temperature increase measured is only ∼0.05 K. If thermal runaway were the key limitation in this test, one might expect that the heating pre-quench would have been higher or that the higher temperature observed by the local thermometry after quench would have resulted in a significantly lower maximum field. Since neither of these were true, it might indicate that film thickness is less likely to play an important role than surface roughness, at least in this case.

It is noteworthy that the cavities were all treated with a N-infusion step, but no excess of N was found in the near surface of a witness sample using SIMS in comparison to a non-infused sample. This may suggest that the N-infusion was not the key factor in performance improvement. Continued studies without this step will help to evaluate its importance.

The high temperature nucleation step appears to help with uniformity and density of coverage of islands early in the coating process, based on sample host cavity studies in the supplemental material. This is expected to help prevent the growth of pachy regions. On the other hand, it is not yet clear what the key factors are that contributed to the formation of smooth, thin coatings—this is a focus of continued investigations. If these investigations lead to consistent achievement of gradients >20 MV m^{-1} in Nb_3Sn cavities, it would be extremely beneficial for accelerator applications.

The films under study in these experiments are bulk films (i.e. thick compared to the penetration depth). There have been concerns in the SRF community about flux penetration at fields above the lower critical field into bulk superconductors that, like Nb_3Sn, have coherence length significantly smaller than Nb, and therefore may be vulnerable to flux entering at small defects. This has led to efforts to develop multilayer coatings with insulating films between superconducting layers to prevent dendritic flux avalanches [48, 49]. The single cell 1.3 GHz cavity (CBMM-D) reached a peak surface magnetic field of approximately 95 mT, well above the expected lower critical field of Nb_3Sn [29, 50, 51], strengthening previous assertions that bulk Nb_3Sn cavities can be maintained in the metastable flux-free state [52]. The small coherence length of Nb_3Sn and

the presence of small-scale defects in realistic films may eventually make multilayer films advantageous, but the experiments presented here demonstrate that Nb_3Sn films in bulk form can reach fields that are sufficiently large for many SRF applications. Furthermore, if it is determined that film smoothness and/or reduced layer thickness are the key factors in the performance presented in this paper, then continued progress in accelerating gradient in Nb_3Sn bulk films may be enabled by further modification of coating and post-processing steps to improve these factors.

6. Conclusions

With the single cell 1.3 GHz cavity, the single cell 650 MHz cavity, and the two 9-cell 1.3 GHz cavities, significant progress is reported on Nb_3Sn SRF cavity development in this paper:

- A record cw accelerating gradient of 24 MV m^{-1} for a cavity made with an SRF material other than Nb, significantly higher than the previous highest cw gradient for a Nb_3Sn cavity ~18 MV m^{-1}
- Two cavities that exhibit $Q_0 > 1 \times 10^{10}$ at 20 MV m^{-1} and 4.4 K, showing promising performance levels for Nb_3Sn in cryocooler-based compact accelerator applications as well as larger-scale accelerator applications where cryogenics are a cost driver;
- $Q_0 \sim 9 \times 10^9$ at 15 MV m^{-1} and 4.4 K on a practical cavity structure commonly used in accelerators;
- First demonstration of multipacting being processed in Nb_3Sn cavities.

These cavities all had shiny surfaces, atypical for Nb_3Sn. Microstructural analysis shows that the shiny films are smoother and thinner than matte films, possibly leading to higher maximum fields due to reduced vulnerability to flux penetration at dips and grooves and/or improved thermal stability. Future work will focus on achieving strong reproducibility, continued progress in maximum field, and further steps towards first applications.

Acknowledgments

The authors are grateful for the dedicated efforts of the SRF processing team at FNAL and ANL, the FNAL VTS testing team, and the FNAL machine shop and welding experts. Thanks also for helpful discussions with Anna Grassellino, Sergey Belomestnykh, Hasan Padamsee, Curtis Crawford, Chuck Grimm, Matthias Liepe, Grigory Eremeev, Daniel Hall, Ryan Porter, Uttar Pudasaini, and the FNAL SRF science team. This manuscript has been authored by Fermi Research Alliance, LLC under Contract No. DE-AC02-07CH11359 with the U.S. Department of Energy, Office of Science, Office of High Energy Physics and supported by the primary author's DOE Early Career Award. This work made use of the EPIC, Keck-II, and/or SPID facilities of Northwestern University's NU*ANCE* Center, which received support from the Soft and Hybrid Nanotechnology Experimental (SHyNE) Resource (NSF ECCS-1542205); the MRSEC program (NSF DMR-1121262) at the Materials Research Center; the International Institute for Nanotechnology (IIN); the Keck Foundation; and the State of Illinois, through the IIN.

ORCID iDs

S Posen https://orcid.org/0000-0002-6499-306X
J Lee https://orcid.org/0000-0001-8542-9612

References

[1] Posen S and Hall D L 2017 Nb_3Sn superconducting radiofrequency cavities: fabrication, results, properties, and prospects *Supercond. Sci. Technol.* **30** 033004
[2] Grassellino A *et al* 2018 Accelerating fields up to 49 MV m^{-1} in TESLA-shape superconducting RF niobium cavities via 75C vacuum bake (arXiv: 1806.09824)
[3] Arnolds-Mayer G and Chiaveri E 1986 On a 500 MHz single cell cavity with Nb_3Sn surface. *Proc. of The Third Workshop on RF Superconductivity*
[4] Peiniger M, Hein M, Klein N, Müller G, Piel H and Thuns P 1988 Work on Nb_3Sn cavities at Wuppertal *Proc. of The Third Workshop on RF Superconductivity*
[5] Hillenbrand B, Martens H, Pfister H, Schnitzke K and Uzel Y 1977 Superconducting Nb_3Sn cavities with high microwave qualities *IEEE Trans. Magn.* **13** 491–5
[6] Kneisel P, Stoltz O and Halbritter J 1977 Nb_3Sn for superconducting RF cavities *Advances in Cryogenic Engineering* (Springer US: Boston, MA) pp 341–6
[7] Transtrum M K, Catelani G and Sethna J P 2011 Superheating field of superconductors within Ginzburg-Landau theory *Phys. Rev.* B **83** 094505
[8] Schneider W J, Kneisel P and Rode C H 2003 Gradient optimization for SC CW accelerators *Proc. Part. Accel. Conf. 2003* 2863–5
[9] Kephart R *et al* 2015 SRF, compact accelerators for industry & society. *Proc. SRF2015*FRBA03
[10] Dhuley R C, Kostin R, Prokofiev O, Geelhoed M I, Nicol T H, Posen S, Thangaraj J C T, Kroc T K and Kephart R D 2019 Thermal link design for conduction cooling of SRF cavities using cryocoolers *IEEE Trans. Appl. Supercond.* **29** 1–5
[11] Ciovati G *et al* 2018 Design of a cw, low-energy, high-power superconducting linac for environmental applications *Phys. Rev. Accel. Beams* **21** 91601
[12] Godeke A 2006 A review of the properties of Nb_3Sn and their variation with A15 composition, morphology and strain state *Supercond. Sci. Technol.* **19** R68–R80
[13] Saur E and Wurm J 1962 Preparation und supraleitungseigenschaften von niobdrahtproben mit Nb_3Sn-Uberzug *Naturwissenschaften* **49** 127–8
[14] Hillenbrand B 1976 Superconducting Nb_3Sn cavities with high quality factors and high critical flux densities *J. Phys. D: Appl. Phys.* **47** 4151
[15] Rudman D A, Hellman F, Hammond R H and Beasley M R 1984 A15 Nb-Sn tunnel junction fabrication and properties *J. Phys. D: Appl. Phys.* **55** 3544–53
[16] Eremeev G, Reece C E, Kelley M J, Pudasaini U and Tuggle J R 2015 Progress with multi-cell Nb_3Sn cavity development linked with sample matierals characterization *Proc. of the Seventeenth Int. Conf. on RF Superconductivity* (*Whistler, Canada*) p TUBA05
[17] Yang Z, He Y, Guo H, Li C, Xiong P, Lu M, Zhang S, Lin Z, Tan T and Zhang S 2019 Development of Nb_3Sn cavity coating at IMP. *Proc. Ninteenth Int. Work. RF Supercond.* (*Dresden, Germany*)

[18] Trenikhina Y, Posen S, Romanenko A, Sardela M, Zuo J, Hall D L and Liepe M 2018 Performance-defining properties of Nb 3 Sn coating in SRF cavities *Supercond. Sci. Technol.* **31** 015004

[19] Lee J, Posen S, Mao Z, Trenikhina Y, He K, Hall D L, Liepe M and Seidman D N 2019 Atomic-scale analyses of Nb_3Sn on Nb prepared by vapor diffusion for superconducting radiofrequency cavity applications: a correlative study *Supercond. Sci. Technol.* **32** 024001

[20] Spina T, Tennis B M, Lee J, Seidman D N and Posen S 2020 Development and understanding of Nb_3Sn films for radiofrequency applications through a sample-host 9-cell cavity (Arxiv: 2006.13407)

[21] Lee J, Mao Z, He K, Sung Z H, Spina T, Baik S I, Hall D L, Liepe M, Seidman D N and Posen S 2020 Grain-boundary structure and segregation in Nb_3Sn coatings on Nb for high-performance superconducting radiofrequency cavity applications *Acta Mater.* **188** 155–65

[22] Porter R, Hall D L, Liepe M and Maniscalco J 2017 Surface roughness effect on the performance of Nb_3Sn cavities *28th Linear Accel. Conf. (LINAC 2016)* (*East Lansing, MI, USA*, *25–30 September 2016*) pp 129–32

[23] Cody G D and Cohen R W 1964 Thermal conductivity of Nb_3Sn *Rev. Mod. Phys.* **36** 121–3

[24] Hall D L 2017 *New Insights into the Limitations on the Efficiency and Achievable Gradients in Nb_3Sn SRF Cavities* Cornell University

[25] Mucklejohn S and O'Brien N 1987 The vapour pressure of tin(II) chloride and the standard molar Gibbs free energy change for formation of $SnCl_2$(g) from Sn(g) and Cl_2(g) *J. Chem. Thermodyn.* **19** 1079–85

[26] Hillenbrand B 1980 The preparation of superconducting Nb_3Sn surfaces for RF applications *Proc. of the First Workshop on RF Superconductivity*

[27] Grassellino A *et al* 2017 Unprecedented quality factors at accelerating gradients up to 45 MVm-1in niobium superconducting resonators via low temperature nitrogen infusion *Supercond. Sci. Technol.* **30** 094004

[28] Posen S and Liepe M 2014 Advances in development of Nb_3Sn superconducting radio-frequency cavities *Phys. Rev. Spec. Top. - Accel. Beams* **17** 112001

[29] Orlando T P, McNiff E J, Foner S and Beasley M R 1979 Critical fields, Pauli paramagnetic limiting, and material parameters of Nb_3Sn and V_3Si *Phys. Rev.* B **19** 4545–61

[30] Kubo T 2017 Multilayer coating for higher accelerating fields in superconducting radio-frequency cavities: a review of theoretical aspects *Supercond. Sci. Technol.* **30** 023001

[31] Rost M J, Quist D A and Frenken. J W M 2003 Grains, growth, and grooving *Phys. Rev. Lett.* **91** 1–4

[32] Melo L L, Vaz A R, Salvadori M C and Cattani M 2004 Grain sizes and surface roughness in platinum and gold thin films *J. Metastable Nanocryst. Mater.* **20–21** 623–8

[33] Pudasaini U, Eremeev G V, Reece C E, Tuggle J and Kelley M J 2018 Effect of deposition temperature and duration on Nb_3Sn diffusion coating *Ninth Int. Part. Accel. Conf.* (*Vancouver, BC, Canada*) THPAL130

[34] Padamsee H, Knobloch J and Hays T 2008 *RF Superconductivity for Accelerators* (Wiley-VCH: New York)

[35] Müller G, Piel H, Pouryamout J, Boccard P and Kneisel P 2000 Status and prospects of Nb_3Sn cavities for superconducting linacs *Proc. of the Workshop on Thin Film Coating Methods for Superconducting Accelerating Cavities*

[36] Ylä-Oijala P 1999 Electron multipacting in TESLA cavities and input couplers *Part. Accel.* **63** 105–37

[37] Altarelli Massimo *et al* 2006 XFEL: The European X-Ray Free-Electron Laser. Technical design report (DESY) pp 2006–097

[38] Galayda John N *et al* Petit-Jean-Genaz Christine, Arduini Gianluigi, Michel Peter and RW Schaa Volker 2014 The linac coherent light source-II project *Proceedings of the Fifth International Particle Accelerator Conference Dresden, Germany* JACoW TUOCA01

[39] Eremeev G, Clemens W, Macha K, Reece C E, Valente-Feliciano A M, Williams S, Pudasaini U and Kelley M 2020 Nb_3Sn multicell cavity coating system at JLAB *Rev. Sci. Instr.* 073911

[40] Eremeev G, Clemens W, Macha K, Reece C E, Valente-Feliciano A M, Williams S, Pudasaini U and Kelley M 2020 Nb_3Sn multicell cavity coating system at Jefferson Lab *Rev. Sci. Instrum.* **91** 073911

[41] Shemelin V and Padamsee H 2008 Magnetic field enhancement at pits and bumps on the surface of superconducting cavities *Telsa Technol. Collab. Rep. 2008-07*

[42] Kubo T 2015 Magnetic field enhancement at a pit on the surface of a superconducting accelerating cavity *Prog. Theor. Exp. Phys.* **2015** 1–16

[43] Pack A R, Carlson J, Wadsworth S and Transtrum M K 2020 Vortex nucleation in superconductors within time-dependent Ginzburg-Landau theory in two and three dimensions: role of surface defects and material inhomogeneities *Phys. Rev.* B **101** 1–10

[44] Aad G *et al* 2012 Observation of a new particle in the search for the standard model Higgs boson with the ATLAS detector at the LHC *Phys. Lett.* B **716** 1–29

[45] Xie Y and Liepe M 2013 Quench and field dependent surface resistance studies using a single cell cavity with artificial pits *Proc. Sixt. Conf. RF Supercond.* (*Paris, France*) TUIOA05

[46] Koechlin F and Bonin B 1996 Parametrization of the niobium thermal conductivity in the superconducting state *Supercond. Sci. Technol.* **9** 453–60

[47] Posen S 2015 Understanding and overcoming limitation mechanisms in Nb_3Sn superconducting RF cavities (Cornell University)

[48] Gurevich A 2006 Enhancement of rf breakdown field of superconductors by multilayer coating *Appl. Phys. Lett.* **88** 012511

[49] Gurevich A 2015 Maximum screening fields of superconducting multilayer structures *AIP Adv.* **5** 017112

[50] Godeke A 2005 Performance boundaries in Nb_3Sn superconductors (The Netherlands: University of Twente, Enschede)

[51] Keckert S *et al* 2019 Critical fields of Nb_3Sn prepared for superconducting cavities *Supercond. Sci. Technol.* 075004

[52] Posen S, Liepe M and Hall D L 2015 Proof-of-principle demonstration of Nb_3Sn superconducting radiofrequency cavities for high Q_0 applications *Appl. Phys. Lett.* **106** 082601